PCCP

PAPER

View Article Online
View Journal | View Issue

Cite this: *Phys. Chem. Chem. Phys.*, 2022, **24**, 15749

Received 20th April 2022,
Accepted 25th May 2022

DOI: 10.1039/d2cp01822e

rsc.li/pccp

Topological bands in the $PdSe_2$ pentagonal monolayer†

Sergio Bravo,[a] M. Pacheco, *[a] J. D. Correa [b] and Leonor Chico [c]

The electronic structure of monolayer pentagonal palladium diselenide ($PdSe_2$) is analyzed from the topological band theory perspective. Employing first-principles calculations, effective models and symmetry indicators, we find that the low-lying conduction bands are topologically nontrivial, protected by time reversal and crystalline symmetries. Numerical evidence supporting the nontrivial character of the bands is presented. Furthermore, we obtain a relevant physical response from the topological viewpoint, such as the spin Hall conductivity.

1 Introduction

Two-dimensional (2D) materials are among the most promising types of systems in the continuous search for novel structures that can give shape to future technological advances. The low-dimensional character of these structures makes them ideal candidates for their application in nanoscale devices.[1] Starting with graphene more than a decade ago, a vast number of these layered systems have been proposed.[2–4] Within this emerging group of novel 2D systems, pentagonal 2D materials are attracting increasing attention because of their symmetry. For instance, the proposal of pentagraphene has stirred much attention.[5–8] Furthermore, the possibility of presenting topologically nontrivial phases has driven the interest towards other pentagonal layers with different compositions.[9–12] However, some theoretical proposals have been shown to be structurally unstable, especially those with dominant p-orbital bonds.[13,14] Notwithstanding, there are several instances of experimentally found 2D pentamaterials, such as $PdSe_2$, PdS_2 and NiN_2.[15–17] Among these, the recently synthesized $PdSe_2$ has been the subject of intensive experimental and theoretical research. Importantly, the pentagonal phase is the stable allotrope for this material. Different forms of pentagonal $PdSe_2$ with a variable number of layers have been reported, possessing high stability in air,[18–22] which is an essential characteristic for their extended (long-term) use. Also, electrical transport characteristics,[23] remarkable optical,[24–27] and good thermoelectric properties[28] have been experimentally reported. On the theoretical side, several works have analyzed the physical properties of the material in its monolayer and multilayer forms.[29–33] Among these theoretical accounts the band connectivity and the symmetry-related properties of the electronic structure have not been studied in detail for monolayer $PdSe_2$; we address this issue in this work. Using the theory of symmetry indicators along with first-principles calculations, we identify that the lowest conduction bands of monolayer $PdSe_2$ realize a topologically nontrivial phase. These bands comprise a strong topological phase with a well defined topological invariant and gapless edge states that we characterize using well-known numerical methods. Also, an analysis of the accessibility of these nontrivial conduction states by Fermi level manipulation is presented. These results open the possibility for the exploration of this promising material and its related structures from the topological point of view.

The article is organized as follows. First, an overview of the numerical calculations and parameters used is sketched. This is followed by the geometric information and first-principles electronic band structure of monolayer $PdSe_2$, along with a study of the symmetry character of the bands. Additionally, effective models based on the Wannier interpolation are briefly described and put forward to study the edge states and the Wannier charge center (WCC) evolution along different directions. The spin Hall conductivity, a signature of its nontrivial band character, is computed as a function of frequency and chemical potential. Finally, we conclude with a summary and outlook for possible future avenues to explore the potential of this material. Part of our results are provided in the ESI.†

[a] *Departamento de Física, Universidad Técnica Federico Santa María, Valparaíso, Chile. E-mail: monica.pacheco@usm.cl*
[b] *Facultad de Ciencias Básicas, Universidad de Medell n, Medell n, Colombia*
[c] *Departamento de Física de Materiales, Facultad de Ciencias Físicas, Universidad Complutense de Madrid, 28040 Madrid, Spain*

† Electronic supplementary information (ESI) available: The topological invariant extraction from the symmetry indicators of space group #14. Additional figures as well as formulae of physical quantities calculated and presented in the main text, such as the shift current and the spin Hall conductivity. See DOI: https://doi.org/10.1039/d2cp01822e

2 Computational details

The calculations for the band structure were carried out with the standard density functional theory (DFT) method using the QUANTUM ESPRESSO (QE) package[34] at the GGA (generalized gradient approximation) level within the Perdew–Burke–Ernzerhof (PBE) implementation. We have also corroborated the robustness of our main results by resorting to the GPAW code[35,36] and checking for several DFT functionals; these additional computations are summarized in Appendix A. The monolayer structure was relaxed with a force tolerance of 10^{-4} eV Å^{-1}. The energy cutoff for the plane wave basis was 100 Ry with a vacuum distance of 20 Å in the perpendicular direction to the monolayer. A Monkhorst–Pack grid of 15 × 15 × 1 was chosen and the energy convergence tolerance was set to 10^{-8} Ry. The Wannier interpolation of the DFT energy bands was performed using the Wannier90 code.[37] Two models were implemented: a twelve-band (12B) model including the four uppermost valence band and the eight lowest conduction bands, and an eight-band (8B) model that only includes the above-mentioned conduction bands. This latter model was used to focus only on the nontrivial bands of the system. For the 12B model, d-orbitals were used for the Pd atoms and p-orbitals for the Se atoms. These orbitals were only used as starting sites for the orbitals since the location of the Wannier centers may change under the wannierization process. The post-processing of Wannier-based models was carried by the PythTB code.[38] Also, Wannier90 was used to analyze this model and to calculate the optical responses presented below. The mathematical expressions implemented in this code are based on ref. 39 and 40, and for quick reference are presented in the ESI.†

3 Electronic band structure and symmetry indicators

3.1 Lattice geometry and space group

The lattice structure of $PdSe_2$ is composed of irregular (type 2) pentagons forming a buckled geometry as presented in Fig. 1(a).[41] Pd atoms are fourfold coordinated and Se atoms have coordination three. As previous studies reported,[18] the crystalline order conforms to a tetragonal lattice, with three symmetry operations: a twofold rotation around one of the lattice vectors axis with fractional translation (1/2,1/2,0) in terms of the unit cell vectors, a mirror glide plane and spatial inversion.[42] This has to be complemented with the time reversal (TR) symmetry to give the space group (SG) $P2_1c$ or SG #14. The Pd atoms sit at the 2*a* Wyckoff position (WP) while the Se atoms locate at the 4*e* WP.[42] The relaxed structure obtained from first-principles calculations comprises a rectangular unit cell with lattice vectors with magnitude a = 5.74 Å and b = 5.91 Å. The calculation also yields a puckering distance of 0.7 Å, confirming the buckled geometry of the material. These results show a good agreement with the reported experimental and theoretical values.[18,29,33,43]

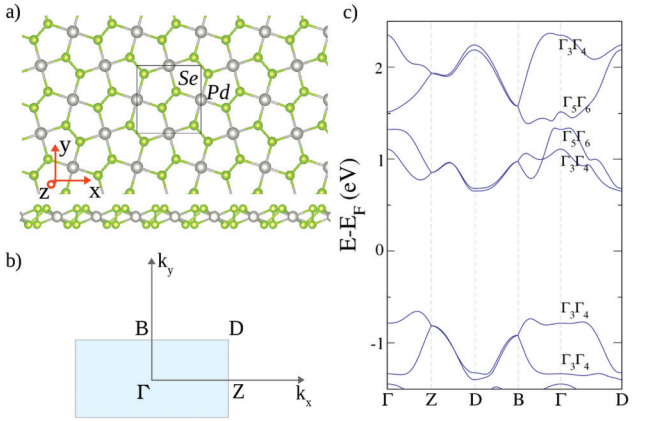

Fig. 1 (a) Lattice structure of monolayer $PdSe_2$. (b) Brillouin zone for the space group #14. (c) Electronic band structure of monolayer $PdSe_2$ along a high-symmetry path. Band energies are with reference to the Fermi level E_F.

The band structure of monolayer $PdSe_2$ has been extensively studied in previous literature.[18,29–33,43] As indicated above, we have also carried out an extensive investigation of its electronic properties by employing several exchange–correlation functionals, detailed in Appendix A. We confirm the robustness of the nontrivial topology found for this material.

Here we focus on the band connectivity and associated topological properties of the low-energy bands around the Fermi level. For this purpose we present in Fig. 1c the electronic band structure including spin–orbit coupling (SOC) at the PBE level along the high-symmetry path *Γ–Z–D–B–Γ–D* in momentum space. The Brillouin zone is depicted in Fig. 1b, following the notation of ref. 44.

The inclusion of SOC is crucial for the results obtained as will be clarified in what follows. It is well-known that PBE functionals systematically underestimate the fundamental gap in semiconductors and insulators. As stated above, we verified that other functionals yield similar results and predict the nontrivial topology found with QE, as detailed in the appendix. Additionally, we have revised the existing literature concerning the electronic structure of monolayer $PdSe_2$ obtained using the hybrid (HSE06) functional[30] and at the GW level.[45] These more expensive calculations show a larger band gap but also keep the band general features unaltered, giving validity for the topological analysis using the PBE functional presented here.

From the band structure and the space group information it can be confirmed that all bands are doubly degenerate along the whole Brillouin zone (BZ) since monolayer $PdSe_2$ is centrosymmetric (SG#14). The spin–orbit interaction – which requires the use of double space groups – obviously affects the degeneracies of the system without SOC, only leaving the possibility of fourfold nodal points at the *Z* and *B* points. These points are protected by the nonsymmorphic symmetries of the SG in conjunction with the time-reversal symmetry,[46] and they are present in every group of four bands in the structure. This is the basic ingredient for the band connectivity of the system, since these sets of four bands form a band representation,[47] following the prescription of topological quantum chemistry theory and symmetry-based indicators.[48–50]

Table 1 Elements of the EBR matrix for the two-dimensional SG#14

IR/EBR	EBR1	EBR2	EBR3	EBR4
$\Gamma_3\Gamma_4$	2	2	0	0
$\Gamma_5\Gamma_6$	0	0	2	2
D_3	1	0	1	0
D_4	1	0	1	0
D_5	0	1	0	1
D_6	0	1	0	1
Z_2	1	1	1	1
B_2	1	1	1	1

The first step in the study of the topological properties of monolayer $PdSe_2$ is the identification of nontrivial topology signatures in the corresponding space group, namely, SG#14. Firstly, it is customary to look for a strong topology, since this is the most widely known nontrivial phase. To this end, we employ the results of ref. 51, adapted for the case of a two dimensional BZ. Specifically, a Smith normal form decomposition is applied to the set of elementary band representations (EBR) of the SG. Recall that EBR are the building blocks to construct the bands of atomic insulators and as such, they can be mapped directly to exponentially localized Wannier functions[52] situated at the atomic positions of the material. The procedure is briefly sketched as follows. First an EBR matrix is constructed, including as coefficients the multiplicities of the irreducible representations (IR) at the high-symmetry points of the material (Γ, Z, D and B for our particular case). The elements of the EBR matrix are provided in Table 1 (using the Bilbao Crystallographic Server information[44]). Next, the Smith normal form matrix Δ is calculated, which is a diagonal matrix with positive integer values. If some of these values are greater that one, then a strong topological phase is possible for the SG.[51] The Δ matrix for the (2D) SG#14 is given by

$$\Delta = \begin{bmatrix} 1 & 0 & 0 & 0 \\ 0 & 1 & 0 & 0 \\ 0 & 0 & 2 & 0 \\ 0 & 0 & 0 & 0 \\ 0 & 0 & 0 & 0 \\ 0 & 0 & 0 & 0 \\ 0 & 0 & 0 & 0 \\ 0 & 0 & 0 & 0 \end{bmatrix}. \quad (1)$$

We observe that a diagonal element with value 2 is present, which allows for a $\mathbb{Z}_2$ phase in the system.[51] Thus, strong topological bands are, in principle, possible in this SG. This phase is a version of the time-reversal plus inversion topological phase,[53] which in this case is further enriched by the other crystalline symmetries of the group. The presence of these additional symmetries simplifies the symmetry-indicated character of the nontrivial topology. This can be seen in the definition of

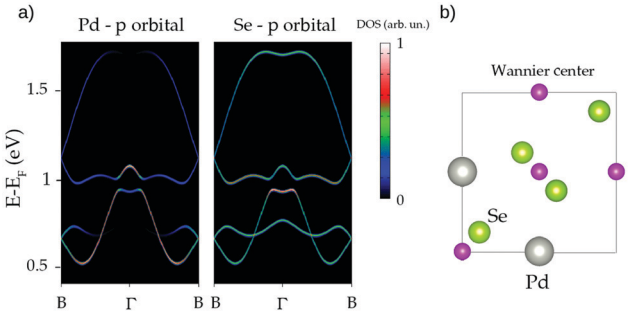

Fig. 2 (a) Orbital-projected bands for monolayer $PdSe_2$. (b) Relative position of the Wannier centers within the unit cell of monolayer $PdSe_2$.

the above mentioned $\mathbb{Z}_2$ invariant. Further manipulation of the EBR matrix (see the ESI† for this particular group or ref. 51 for the general theory) gives the result that the $\mathbb{Z}_2$ invariant only depends on the parity of the Γ point IR. In this double SG Γ only has two IR, $\Gamma_3\Gamma_4$ and $\Gamma_5\Gamma_6$.[54] With this definition the topological invariant for the strong phase can be defined as

$$\mathbb{Z}_2 = n_{\Gamma_3\Gamma_4} (\mathrm{mod}\ 2) = n_{\Gamma_5\Gamma_6} (\mathrm{mod}\ 2), \quad (2)$$

where $n_{\Gamma_3\Gamma_4}$ and $n_{\Gamma_5\Gamma_6}$ correspond to the multiplicities of the IR at Γ. In other words, if a single (fourfold) band representation or a group of band representations has an odd number of $\Gamma_3\Gamma_4/\Gamma_5\Gamma_6$ IR, then these bands are topological. This definition of $\mathbb{Z}_2$ is simpler than the standard Fu-Kane formula for TR inversion-symmetric insulators[55] due to the additional constraints of the above-mentioned symmetries. Note that this is the only kind of symmetry-indicated topology that can be present in this two-dimensional (layer) version of SG#14. The linear combination of strong band representations may yield either a strong band or a trivial band representation. This differs from the three-dimensional version of this group, where fragile bands and strong bands can coexist.[51] We have numerically computed the IR characters for monolayer $PdSe_2$ from the first-principles electronic structure using the IrRep package.[56] We consider two groups of bands: the valence band manifold of the material and the eight lowest conduction bands. In the valence band set there exists an even number of $\Gamma_3\Gamma_4/\Gamma_5\Gamma_6$ irreducible representations, which render the material a trivial insulator. On the other hand, if we take into account the aforementioned conduction bands, we find that both fourfold band representations have separately an odd number of $\Gamma_3\Gamma_4/\Gamma_5\Gamma_6$ IR. Therefore, each single group realizes a strong topological group of bands. In Fig. 1c) we have labeled the highest valence band and the lowest conduction bands with the corresponding IR. A crucial role here is played by the SOC, which permits a band inversion between the two groups of band representations. The inversion can be initially identified from the band structure in Fig. 1c, specially along the B–Γ line. Further confirmation of this band inversion is presented in Fig. 2a, where the orbital-projected bands are presented. The p-orbitals constitute the most important contribution to the inversion and the effective models for these bands are based on this result.

3.2 Evidence of the nontrivial topology

A clearer picture of the nontrivial topology of monolayer $PdSe_2$ can be obtained by the computation of the standard quantities that pinpoint the nontrivial character of the bands. Thus, we calculated the energy dispersion for a ribbon geometry of the material and the bulk Wannier charge center (WCC) evolution along the BZ,[57] using a Wannier-based model. Before delving into these results, we would like to comment on the Wannier centers in real space associated with the conduction bands. We employed a reduced 8B model, as described above, to account only for these bands. They are well separated from the higher conduction bands, which make them suitable for faithful wannierization. The localization of the Wannier centers in real space for $PdSe_2$ is represented in Fig. 2b). A pair of Wannier centers sits on each site, as dictated by time reversal symmetry (Kramers pairs).[58] Most importantly, it can be observed that two pairs of these Wannier centers are localized at a WP (2b) that is not occupied by any of the atoms in the material. This *obstruction* hints for a nontrivial topology[58] and $PdSe_2$ can be dubbed as a conduction-band-obstructed atomic insulator. The other Wannier centers localize on the 2a WP and thus coincide with atomic (Pd) orbitals. The WCC evolution along the k_x direction in the BZ is presented in Fig. 3a. Here we also use the 8B model in order to isolate the nontrivial behavior. For this model we assume that the four lowest conduction bands are occupied, just to conform with the usual WCC definition.[52] The general trend of the WCC evolution shows the typical features of a TR inversion-symmetric topological insulator,[53] with the nontrivial crossings at one of the time-reversal invariant momenta (in this case $k_x = \pi$). The energy dispersion of the edge states for a confined geometry is plotted in Fig. 3b). In this case we make use of the 12B model, with the aim to show the fundamental gap and their edge states. Gapless energy states arise within the gap at $\approx$1.3 eV above the Fermi level, localized on the edges of the finite slab, giving further confirmation for the nontrivial phase of the conduction bands. The edge termination has influence on the dispersion of the edge states, but there are always gapless states in this upper gap. The fundamental gap also presents edge states that are trivial in terms of the above classification. Further information for other edges is presented in the ESI.†

4 Topologically relevant physical responses

The main drawback of the topological bands spotted in the above discussion is that they are situated in the conduction bands, which implies that some external manipulation of the material is necessary in order to access them. This hinders the use of monolayer $PdSe_2$ as a spin Hall insulator, since the nontrivial gap is not the fundamental gap. Notwithstanding, the lowest conduction bands of the material are reachable by standard doping and gating.[1,59] Nowadays there are gating techniques for 2D materials which allows for higher doping levels than standard methods.[60,61] As these procedures can displace the chemical potential μ to lie inside the conduction bands, it is possible to access the nontrivial bands and explore the nontrivial behavior of the material. We simulate this electron doping effect by a rigid shift of the chemical potential using the 12B model and calculate an optical response, namely, the frequency-dependent spin Hall conductivity (SHC) for different values of the chemical potential. The slab geometry has been taken into account by a global scaling factor following ref. 39. We report the real part in Fig. 4; only the usual component with spin along the z direction and transverse current with respect to the applied external field is presented. We have calculated cases with the chemical potential within the conduction band and also inside the trivial valence bands to assess the magnitude of the response. Additionally, the SHC with no doping effect is included. It can be appreciated that both types of doping produce a new intense peak in the low-frequency range of the spectrum. However, when μ is situated around the nodal features of the conduction bands – around 1 eV above the original Fermi level – the magnitude of this peak is greatly enhanced, giving additional support to the nontrivial character of the bands.

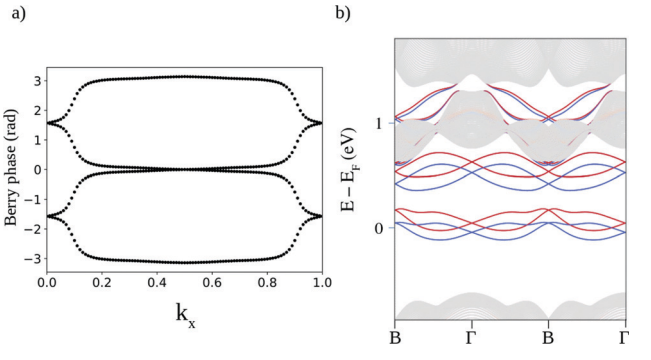

Fig. 3 (a) Evolution of the Wannier charge center (Wilson loop) along the k_x direction. (b) Energy dispersion of the ribbons for the Wannier interpolated 12B model. Red-colored and blue-colored bands represent states that are localized at the upper and lower edges of the ribbon, respectively.

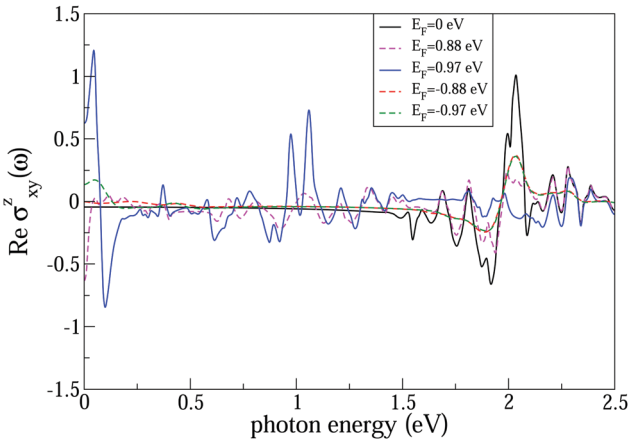

Fig. 4 Real part of the spin Hall conductivity σ^z_{xy} as a function of external photon energy for different chemical potential values.

Although the topological character is not crucial for an enhanced magnitude of the effect, as can be checked by the large static SHC in Pt,[62] it can boost the optical response. Several other studies have reported sizable values for the two-dimensional semiconductors.[63,64] It is important to note that the above-mentioned optical effects could be affected by the inclusion of quasiparticle effects, such as those discussed in ref. 30 for the linear optical response.

Additionally, from Fig. 4 it can be observed that the static limit ($\omega \to 0$) of the optical SHC yields a nonzero value even for the undoped system, implying a nonzero SHC within the fundamental gap. This situation has been encountered in previous calculations of the SHC on semiconductors such as in ref. 65 and 66, where it is mentioned that the in-gap SHC cannot give rise to spin accumulation for trivial systems. Recently,[64] it has been argued that this SHC is only a numerical artifact due to the use of a broadening factor and, by means of degenerate perturbation theory, they obtain zero in-gap conductivities for trivial insulators. For completeness we have computed this static SHC for monolayer $PdSe_2$, using the method of ref. 64 as implemented in ref. 67, and also using the Wannier90 code,[40] which uses the standard broadening factor. In both cases we obtain a constant nonzero value along both the trivial and the nontrivial gaps. Yet, the magnitude in the case of the trivial gap is low and in principle were not detectable. This static SHC is presented in the ESI.†

5 Conclusions

In this work we address the electronic band topology of monolayer $PdSe_2$. We have shown that, although the valence bands of the material are trivial and in principle the system is a trivial topological insulator, the lowest conduction bands have a nontrivial topology. By means of standard analysis we have found that the group of lowest fourfold-degenerated conduction bands are separately nontrivial, characterized by a $\mathbb{Z}_2 = 1$ invariant. This phase is strong and gives rise to gapless edge states in the conduction band gap and to a nontrivial WCC evolution. The nontrivial character of these bands is in principle accessible by doping, and we have presented numerical evidence for enhanced responses in the case of the optical spin Hall conductivity at low frequency. It can be mentioned that other materials with the same pentagonal structure and space group in the monolayer form has been theoretically reported in several computational databases.[68,69] Many of these materials – such as for example $PtTe_2$, $PdTe_2$ and $NiTe_2$ – show a similar behavior for the low-lying conduction bands and are expected to host similar nontrivial bands. Further work is also needed to elucidate other connections between the nontrivial bands and physical responses not covered here. Additionally, topological bands could likely be present in multilayer $PdSe_2$ and their effects for the low energy regime are worth being explored.

Conflicts of interest

There are no conflicts of interest to declare.

Appendix: electronic characterization of $PdSe_2$ monolayer

In this section we present the theoretical electronic characterization of the $PdSe_2$ monolayer, *i.e.*, the electronic band structure computed within a first-principles approach with different exchange–correlation functionals. The calculations are performed in the framework of density functional theory (DFT) as implemented in GPAW using several GGA and van der Waals (vdW) exchange–correlation functionals.[35,36] A projected augmented wave (PAW) method was employed for the basis set with an energy cutoff of 650 eV. For the *k*-points we used a grid of $15 \times 15 \times 1$. All structures are fully relaxed until the atomic forces in each atom were less than 0.02 eV $Å^{-1}$.

The computed values of the lattice constants and the band-gap of the 2D pentagonal $PdSe_2$ are shown in Table 2. Compared

Table 2 Obtained structural parameters and band gap of $PdSe_2$ monolayer employed different exchange–correlation functionals

XC	*a* (Å)	*b* (Å)	Gap (eV)	Group #
PBE	5.84960	5.90720	1.108	14
LDA	5.73997	5.78863	1.171	14
RPBE	5.89355	5.95226	1.086	14
revPBE	5.88490	5.93966	1.094	14
vdW-DF	5.96822	6.04448	0.943	14
vdW-DF2	6.03519	6.03519	0.850	14
optPBE-vdW	5.90887	5.98340	0.976	14
C09-vdW	5.82330	5.89056	1.025	14
GLLBSC			1.880	
exp-bulk[15]	5.7457	5.8679		

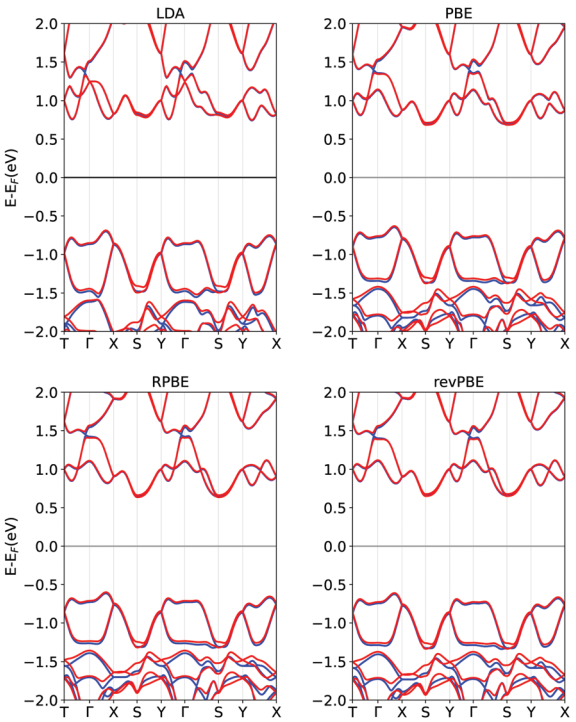

Fig. 5 Band structures of $PdSe_2$ monolayer. Each panel represents a different GGA exchange–correlation functional. Red bands include SOC; blue bands are computed without SOC.

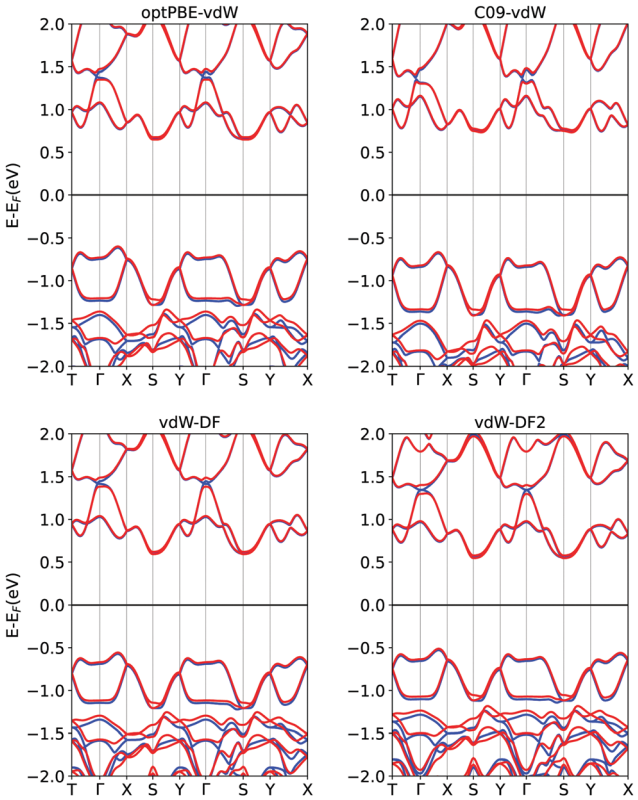

Fig. 6 Band structures of $PdSe_2$ monolayer. Each panel represents a different vdW functional. Red bands include SOC; blue bands are computed without SOC.

to the experimental values for bulk $PdSe_2$ reported in ref. 15, we observe that the PBE functional shows a maximum difference of 0.05 Å for the *b* lattice parameter. If vdW interactions are considered, the maximum difference in the lattice constant is 0.26 Å for the vdW-DF2 functional, in agreement with a previous report of theoretical lattice parameters of bulk $PdSe_2$.[15] Independently of the geometric configuration obtained for every exchange–correlation functional, the symmetry group of monolayer $PdSe_2$ is preserved.

The band structures for $PdSe_2$ monolayer are shown in Fig. 5 and 6. The *k*-point path is labeled using the high-symmetry points of the 3D orthorhombic lattice. Our results show that, independently of the exchange–correlation functional, the topology characteristics of the bands are preserved and are the same as those obtained with QE calculations.

Acknowledgements

This work has been partially supported by the Chilean FONDECYT Grant 1211913, Spanish MCIU and AEI and the European Union under Grant No. PGC2018-097018-B-I00 (MCIU/AEI/FEDER, UE), and by Grant USM-DGIIP PI-LI 1925.

References

1 G. Fiori, F. Bonaccorso, G. Iannaccone, T. Palacios, D. Neumaier, A. Seabaugh, S. K. Banerjee and L. Colombo, *Nat. Nanotechnol.*, 2014, **9**, 768–779.
2 P. Miró, M. Audiffred and T. Heine, *Chem. Soc. Rev.*, 2014, **43**, 6537–6554.
3 D. Saptarshi, J. A. Robinson, M. Dubey, H. Terrones and M. Terrones, *Annu. Rev. Mater. Res.*, 2015, **45**, 1–27.
4 K. Novoselov, A. Mishchenko, A. Carvalho and A. H. Castro Neto, *Science*, 2016, **353**, 461.
5 C.-P. Tang, S.-J. Xiong, W.-J. Shi and J. Cao, *J. Appl. Phys.*, 2014, **115**, 113702.
6 S. Zhang, J. Zhou, Q. Wang, X. Chen, Y. Kawazoe and P. Jena, *Proc. Natl. Acad. Sci. U. S. A.*, 2015, **112**, 2372–2377.
7 S. Bravo, J. Correa, L. Chico and M. Pacheco, *Sci. Rep.*, 2018, **8**, 11070.
8 J. Correa, M. Pacheco, S. Bravo and L. Chico, *Carbon*, 2020, **162**, 209–219.
9 T. Zhao, S. Zhang, Y. Guo and Q. Wang, *Nanoscale*, 2016, **8**, 233–242.
10 H. L. Zhuang, *Comput. Mater. Sci.*, 2019, **159**, 448–453.
11 S. Bravo, J. Correa, L. Chico and M. Pacheco, *Sci. Rep.*, 2019, **9**, 12754.
12 S. Bravo, M. Pacheco, V. Nuñez, J. D. Correa and L. Chico, *Nanoscale*, 2021, **13**, 6117–6128.
13 P. Avramov, V. Demin, M. Luo, C. H. Choi, P. B. Sorokin, B. Yakobson and L. Chernozatonskii, *J. Phys. Chem. Lett.*, 2015, **6**, 4525–4531.
14 A. V. Kuklin, H. Ågren and P. V. Avramov, *Phys. Chem. Chem. Phys.*, 2020, **22**, 8289–8295.
15 A. D. Oyedele, S. Yang, L. Liang, A. A. Puretzky, K. Wang, J. Zhang, P. Yu, P. R. Pudasaini, A. W. Ghosh, Z. Liu, C. M. Rouleau, B. G. Sumpter, M. F. Chisholm, W. Zhou, P. D. Rack, D. B. Geohegan and K. Xiao, *J. Am. Chem. Soc.*, 2017, **139**, 14090–14097.
16 X. Zhang, G. Su, J. Lu, W. Yang, W. Zhuang, K. Han, X. Wang, Y. Wan, X. Yu and P. Yang, *ACS Appl. Mater. Interfaces*, 2021, **13**, 43063–43074.
17 M. Bykov, E. Bykova, A. V. Ponomareva, F. Tasnádi, S. Chariton, V. B. Prakapenka, K. Glazyrin, J. S. Smith, M. F. Mahmood, I. A. Abrikosov and A. F. Goncharov, *ACS Nano*, 2021, **15**, 13539–13546.
18 A. D. Oyedele, S. Yang, L. Liang, A. A. Puretzky, K. Wang, J. Zhang, P. Yu, P. R. Pudasaini, A. W. Ghosh, Z. Liu, C. M. Rouleau, B. G. Sumpter, M. F. Chisholm, W. Zhou, P. D. Rack, D. B. Geohegan and K. Xiao, *J. Am. Chem. Soc.*, 2017, **139**, 14090–14097.
19 G. D. Nguyen, A. D. Oyedele, A. Haglund, W. Ko, L. Liang, A. A. Puretzky, D. Mandrus, K. Xiao and A.-P. Li, *ACS Nano*, 2020, **14**, 1951–1957.
20 M. Fu, L. Liang, Q. Zou, G. D. Nguyen, K. Xiao, A.-P. Li, J. Kang, Z. Wu and Z. Gai, *J. Phys. Chem. Lett.*, 2020, **11**, 740–746.
21 C. Xie, S. Jiang, Y. Gao, M. Hong, S. Pan, J. Zhao and Y. Zhang, *Small*, 2020, **16**, 2000754.
22 L.-S. Lu, G.-H. Chen, H.-Y. Cheng, C.-P. Chuu, K.-C. Lu, C.-H. Chen, M.-Y. Lu, T.-H. Chuang, D.-H. Wei, W.-C. Chueh, W.-B. Jian, M.-Y. Li, Y.-M. Chang, L.-J. Li and W.-H. Chang, *ACS Nano*, 2020, **14**, 4963–4972.
23 A. D. Oyedele, S. Yang, T. Feng, A. V. Haglund, Y. Gu, A. A. Puretzky, D. Briggs, C. M. Rouleau, M. F. Chisholm,

R. R. Unocic, D. Mandrus, H. M. Meyer, S. T. Pantelides, D. B. Geohegan and K. Xiao, *J. Am. Chem. Soc.*, 2019, **141**, 8928–8936.
24 J. Yu, X. Kuang, Y. Gao, Y. Wang, K. Chen, Z. Ding, J. Liu, C. Cong, J. He, Z. Liu and Y. Liu, *Nano Lett.*, 2020, **20**, 1172–1182.
25 J. Yu, X. Kuang, J. Li, J. Zhong, C. Zeng, L. Cao, Z. Liu, Z. Zeng, Z. Luo, T. He, A. Pan and Y. Liu, *Nat. Commun.*, 2021, **12**, 1083.
26 X. Chen, J. Huang, C. Chen, M. Chen, G. Hu, H. Wang, N. Dong and J. Wang, *Adv. Opt. Mater.*, 2022, **10**, 2101963.
27 V. K. Gudelli and G.-Y. Guo, *New J. Phys.*, 2021, **23**, 093028.
28 Y. Zhao, P. Yu, G. Zhang, M. Sun, D. Chi, K. Hippalgaonkar, J. T.-L. Thong and J. Wu, *Adv. Funct. Mater.*, 2020, **30**, 2004896.
29 J. Sun, H. Shi, T. Siegrist and D. J. Singh, *Appl. Phys. Lett.*, 2015, **107**, 153902.
30 A. V. Kuklin and H. Ågren, *Phys. Rev. B*, 2019, **99**, 245114.
31 A. V. Kuklin, L. V. Begunovich, L. Gao, H. Zhang and H. Ågren, *Phys. Rev. B*, 2021, **104**, 134109.
32 W. Lei, W. Wang, X. Ming, S. Zhang, G. Tang, X. Zheng, H. Li and C. Autieri, *Phys. Rev. B*, 2020, **101**, 205149.
33 L.-Y. Feng, R. A.-B. Villaos, Z.-Q. Huang, C.-H. Hsu and F.-C. Chuang, *New J. Phys.*, 2020, **22**, 053010.
34 P. Giannozzi, O. Baseggio, P. Bonfà, D. Brunato, R. Car, I. Carnimeo, C. Cavazzoni, S. de Gironcoli, P. Delugas, F. Ferrari Ruffino, A. Ferretti, N. Marzari, I. Timrov, A. Urru and S. Baroni, *J. Chem. Phys.*, 2020, **152**, 154105.
35 J. J. Mortensen, L. B. Hansen and K. W. Jacobsen, *Phys. Rev. B: Condens. Matter Mater. Phys.*, 2005, **71**, 035109.
36 J. Enkovaara, C. Rostgaard, J. J. Mortensen, J. Chen, M. Dułak, L. Ferrighi, J. Gavnholt, C. Glinsvad, V. Haikola, H. A. Hansen, H. H. Kristoffersen, M. Kuisma, A. H. Larsen, L. Lehtovaara, M. Ljungberg, O. Lopez-Acevedo, P. G. Moses, J. Ojanen, T. Olsen, V. Petzold, N. A. Romero, J. Stausholm-Møller, M. Strange, G. A. Tritsaris, M. Vanin, M. Walter, B. Hammer, H. Häkkinen, G. K.-H. Madsen, R. M. Nieminen, J. K. Nørskov, M. Puska, T. T. Rantala, J. Schiøtz, K. S. Thygesen and K. W. Jacobsen, *J. Phys.: Condens. Matter*, 2010, **22**, 253202.
37 A. A. Mostofi, J. R. Yates, G. Pizzi, Y.-S. Lee, I. Souza, D. Vanderbilt and N. Marzari, *Comput. Phys. Commun.*, 2014, **185**, 2309–2310.
38 S. Coh and D. Vanderbilt, Python Tight Binding (PythTB), **https://www.physics.rutgers.edu/pythtb/**.
39 J. Ibañez-Azpiroz, S. S. Tsirkin and I. Souza, *Phys. Rev. B*, 2018, **97**, 245143.
40 J. Qiao, J. Zhou, Z. Yuan and W. Zhao, *Phys. Rev. B*, 2018, **98**, 214402.
41 H. L. Zhuang, *Comput. Mater. Sci.*, 2019, **159**, 448–453.
42 A. P.-C. Christopher Bradley, *The Mathematical Theory of Symmetry in Solids: Representation Theory for Point Groups and Space Groups*, Oxford University Press, Oxford, New York, 2010.
43 W. Lei, B. Cai, H. Zhou, G. Heymann, X. Tang, S. Zhang and X. Ming, *Nanoscale*, 2019, **11**, 12317–12325.
44 M. I. Aroyo, A. Kirov, C. Capillas, J. M. Perez-Mato and H. Wondratschek, *Acta Crystallogr., Sect. A: Found. Crystallogr.*, 2006, **62**, 115–128.
45 H.-g Kim and H. J. Choi, *Phys. Rev. B*, 2021, **103**, 165419.
46 M. S. Dresselhaus, G. Dresselhaus and A. Jorio, *Group Theory: Application to the Physics of Condensed Matter*, Springer-Verlag, Berlin Heidelberg, 2008.
47 J. Cano, B. Bradlyn, Z. Wang, L. Elcoro, M. G. Vergniory, C. Felser, M. I. Aroyo and B. A. Bernevig, *Phys. Rev. B*, 2018, **97**, 035139.
48 J. Cano and B. Bradlyn, *Annu. Rev. Condens. Matter Phys.*, 2021, **12**, 225–246.
49 J. Kruthoff, J. de Boer, J. van Wezel, C. L. Kane and R.-J. Slager, *Phys. Rev. X*, 2017, **7**, 041069.
50 H. C. Po, A. Vishwanath and H. Watanabe, *Nat. Commun.*, 2017, **8**, 50.
51 L. Elcoro, Z. Song and B. A. Bernevig, *Phys. Rev. B*, 2020, **102**, 035110.
52 D. Vanderbilt, *Berry Phases in Electronic Structure Theory: Electric Polarization, Orbital Magnetization and Topological Insulators*, Cambridge University Press, 2018.
53 A. Alexandradinata, X. Dai and B. A. Bernevig, *Phys. Rev. B: Condens. Matter Mater. Phys.*, 2014, **89**, 155114.
54 L. Elcoro, B. Bradlyn, Z. Wang, M. G. Vergniory, J. Cano, C. Felser, B. A. Bernevig, D. Orobengoa, G. de la Flor and M. I. Aroyo, *J. Appl. Crystallogr.*, 2017, **50**, 1457–1477.
55 L. Fu and C. L. Kane, *Phys. Rev. B: Condens. Matter Mater. Phys.*, 2007, **76**, 045302.
56 M. Iraola, J. L. Mañes, B. Bradlyn, T. Neupert, M. G. Vergniory and S. S. Tsirkin, *IrRep: symmetry eigenvalues and irreducible representations of ab initio band structures*, 2020.
57 M. Taherinejad, K. F. Garrity and D. Vanderbilt, *Phys. Rev. B: Condens. Matter Mater. Phys.*, 2014, **89**, 115102.
58 A. A. Soluyanov and D. Vanderbilt, *Phys. Rev. B: Condens. Matter Mater. Phys.*, 2011, **83**, 035108.
59 Q. H. Wang, K. Kalantar-Zadeh, A. Kis, J. N. Coleman and M. S. Strano, *Nat. Nanothecnol.*, 2012, **7**, 699–712.
60 S. Z. Bisri, S. Shimizu, M. Nakano and Y. Iwasa, *Adv. Mater.*, 2017, **29**, 1607054.
61 I. Gutiérrez-Lezama, N. Ubrig, E. Ponomarev and A. F. Morpurgo, *Nat. Rev. Phys.*, 2021, **3**, 508–519.
62 G. Y. Guo, S. Murakami, T.-W. Chen and N. Nagaosa, *Phys. Rev. Lett.*, 2008, **100**, 096401.
63 L. Matthes, S. Küfner, J. Furthmüller and F. Bechstedt, *Phys. Rev. B*, 2016, **94**, 085410.
64 J. Sławińska, F. T. Cerasoli, H. Wang, S. Postorino, A. Supka, S. Curtarolo, M. Fornari and M. B. Nardelli, *2D Mater.*, 2019, **6**, 025012.
65 G. Y. Guo, Y. Yao and Q. Niu, *Phys. Rev. Lett.*, 2005, **94**, 226601.
66 Y. Yao and Z. Fang, *Phys. Rev. Lett.*, 2005, **95**, 156601.
67 M. B. Nardelli, F. T. Cerasoli, M. Costa, S. Curtarolo, R. De Gennaro, M. Fornari, L. Liyanage, A. R. Supka and H. Wang, *Comput. Mater. Sci.*, 2018, **143**, 462–472.
68 S. Haastrup, M. Strange, M. Pandey, T. Deilmann, P. S. Schmidt, N. F. Hinsche, M. N. Gjerding, D. Torelli, P. M. Larsen, A. C. Riis-Jensen, J. Gath, K. W. Jacobsen, J. Jørgen Mortensen, T. Olsen and K. S. Thygesen, *2D Mater.*, 2018, **5**, 042002.
69 K. Choudhary, I. Kalish, R. Beams and F. Tavazza, *Sci. Rep.*, 2017, **7**, 5179.